Seyed Mahmood Mousavi
School of Mechanical Engineering,
Shiraz University,
Shiraz 71936-16548, Iran
e-mail: sm.mousavi@shirazu.ac.ir

Reza Kamali
School of Mechanical Engineering,
Shiraz University,
Shiraz 71936-16548, Iran
e-mail: rkamali@shirazu.ac.ir

Freshteh Sotoudeh
School of Mechanical Engineering,
Shiraz University,
Shiraz 71936-16548, Iran
e-mail: f.sotoudeh@shirazu.ac.ir

Nader Karimi[1]
Research Division of Systems, Power and Energy,
School of Engineering,
University of Glasgow,
Glasgow G12 8QQ, UK
e-mail: Nader.Karimi@glasgow.ac.uk

Bok Jik Lee
Institute of Advanced Aerospace Technology,
Seoul National University,
Seoul 08826, South Korea
e-mail: b.lee@snu.ac.kr

Numerical Investigation of the Plasma-Assisted MILD Combustion of a CH_4/H_2 Fuel Blend Under Various Working Conditions

The effects of plasma injection upon MILD combustion of a mixture of methane and hydrogen are investigated numerically. The injected plasma includes the flow of a highly air-diluted methane including C_2H_2, C_2H_4, C_2H_6, CH, CH_2, CH_3, CO, and CO_2. The results show that among all the constitutes of plasma, CH_3 is the most effective in improving the characteristics of MILD combustion. Injection of this radical leads to the occurrence of reactions at a closer distance to the burner inlet and thus provides longer time for completion of combustion. Further, mass fractions of OH, CH_2O, and HCO are considerably affected by the injections of CH_3, indicating structural modifications of the reacting flow. Importantly, as Reynolds number of the plasma flow increases, the volume and width of the flame decrease, while the formations of prompt and thermal NO_x are intensified. However, injection of CH_3, as plasma, reduces the emission of thermal NO_x.
[DOI: 10.1115/1.4048507]

Keywords: MILD combustion, plasma-assisted reaction, ignition delay, detailed chemical reaction mechanism, methane-hydrogen blends, energy conversion/systems, fuel combustion, hydrogen energy

1 Introduction

Achieving clean and efficient combustion remains as an important industrial priority and therefore continues to attract significant attention [1,2]. Moderate or intense low-oxygen dilution (MILD) [3–5] combustion is a well-demonstrated concept that provides preheating and dilution simultaneously and thus reduces the emissions significantly. Over the past two decades, there has been a sustained interest in MILD combustion and several comprehensive studies on this topic have been already carried out. Recently, the possibility of improving combustion has been demonstrated through taking different approaches [6–10]. This includes utilizing hybridized solar thermal energy and combustion [11–13], novel burner designs [14], swirl injection [15], and changes in the injection parameters [16–19]. In addition to these, the use of plasma actuators by injecting reactive chemical species has allowed achieving more efficient combustion [20]. Given the ability of plasma actuators to assist combustion processes, many researchers have explored different aspects of this method. Some of these efforts are briefly reviewed in the followings.

The impacts of initial conditions on the characteristics of premixed MILD combustion from a single jet burner were investigated numerically and experimentally by Li et al. [21]. The results showed that for the Reynold numbers greater than the critical Reynolds number, a stable MILD combustion could be established regardless of the nozzle cross-sectional surface area, equivalence ratio, and initial dilution of the reactants. Pilla et al. [22] stabilized a turbulent premixed flame and improved its efficiency through using a nanosecond repetitively pulsed plasma. They showed that the plasma significantly increases the heat release and the combustion efficiency when it is placed in the recirculation zone of the flow, thus allowing to stabilize the flame under lean conditions where it would not exist without plasma. Kim et al. [23] numerically studied the laminar premixed flame structure under the effects of plasma actuator. They showed that the nonequilibrium discharge could facilitate burning of lean methane-air mixtures as it acts as an in situ reformer of the fuel and generates primarily H_2 and CO. Sun et al. [24,25] investigated the direct ignition and *S*-curve transition by in situ nanosecond pulsed discharge in dimethyl ether/oxygen/helium mixture and methane/oxygen/helium counterflow flame. They showed that atomic oxygen produced by the plasma discharge has an important role in controlling the process of radical production.

Yin et al. [26] measured the temperature and hydroxyl radical generation as well as the decay in lean fuel–air mixtures excited by a repetitively pulsed nanosecond discharge. These authors found that in C_2H_4-air and C_3H_8-air, OH free radical declines after the plasma discharge on the 0.02–0.1 ms time scale, while this happens in ~0.1–1.0 ms and 0.5–1.0 ms for CH_4-air and H_2-air, respectively. Rousso et al. [27] studied the low temperature oxidation and pyrolysis of n-heptane in nanosecond-pulsed plasma discharges. It was found that increases in the plasma frequency result in changes in the linear trend of n-heptane dissociation and production of species formation in oxidation and pyrolysis. Cheong et al. [28] investigated the premixed MILD combustion and pollutant emissions of a single jet burner in a cylindrical furnace. They observed that with sufficient residence time, an enhanced injection velocity reduces NO emission mainly by growing the flue gas recirculation rate and thus reducing the local peak temperature. A self-consistent framework for modeling and

[1]Corresponding author.

Contributed by the Advanced Energy Systems Division of ASME for publication in the Journal of Energy Resources Technology. Manuscript received March 31, 2020; final manuscript received July 1, 2020; published online October 14, 2020. Assoc. Editor: Samer F. Ahmed.

simulations of plasma-assisted ignition and combustion is established by Yang et al. [29]. They reported that plasma actuator enhances the production of radicals and flame stabilization, while it also increases the heating of reactants in the preheating zone. Counterflow diffusion flame oscillations induced by ns pulse electric discharge waveforms is evaluated with Tang et al. [30] and it is clear that a high peak ionization fraction generated by a ns pulse discharge allows for a better control of the flame.

In recent years, the use of plasma actuator to improve MILD combustion has been investigated. Wada et al. [31] and Ju et al. [32] found that the reforming of a portion of a CH_4/air mixture at the exit of the fuel jet into intermediate species and the resultant flow perturbations caused by the large density gradient have significant impacts on the ignition delay and the mixing process. Mardani and Khanehzar [33] showed that applying the plasma discharge to the flame region leads to an intensification of the reaction zone, increment of heat release rate by a factor of 3, and 30% reduction of flame liftoff. Different aspects of plasma effect through chemical kinetics, mixing, and thermal heating on MILD combustion have been investigated.

The preceding review of literature revealed the significant potentials of plasma actuators in improving MILD combustion. So far, the research efforts have been predominately focused on the evaluation of plasma effects upon the enhancement of heat release and reduction of the ignition delay. As a result, other aspects of the problem such as the way that the flame shape is influenced by the addition of plasma flow have received comparatively less attention. Also, the relation between plasma injection parameters, e.g., its Reynolds number, and formation of NO_x still needs further investigation. The present work aims to address these shortcomings through conduction of a numerical analysis.

2 Governing Equations

Figure 1 shows a schematic view of the configuration considered in the current computational study. The simulated domain is the central plane of a cylindrical region containing a reactive jet, similar to the classical configuration for MILD combustion explained in Ref. [34]. However, as Fig. 1 shows, a plasma actuator is added to the conventional MILD burner through an annulus surrounding the fuel nozzle.

The governing equations for the reactive flow include conservation of mass, momentum, species, and energy that are solved on the central plane shown in Fig. 1. These equations are expressed in cylindrical coordinate as follows.

Conservation of mass:

$$\frac{\partial \rho}{\partial t} + \frac{\partial}{\partial x}(\rho v_x) + \frac{\partial}{\partial r}(\rho v_r) + \frac{\rho v_r}{r} = 0 \tag{1}$$

Flow momentum in the axial direction:

$$\frac{\partial}{\partial t}(\rho v_x) + \frac{1}{r}\frac{\partial}{\partial x}(r\rho v_x v_x) + \frac{1}{r}\frac{\partial}{\partial r}(r\rho v_r v_x) = -\frac{\partial p}{\partial x} + \frac{1}{r}\frac{\partial}{\partial x}\left[r\mu\left(2\frac{\partial v_x}{\partial x} - \frac{2}{3}(\nabla \cdot \mathbf{v})\right)\right] + \frac{1}{r}\frac{\partial}{\partial x}\left[r\mu\left(\frac{\partial v_x}{\partial r} + \frac{\partial v_r}{\partial x}\right)\right] \tag{2}$$

Flow momentum in the radial direction:

$$\frac{\partial}{\partial t}(\rho v_r) + \frac{1}{r}\frac{\partial}{\partial x}(r\rho v_x v_r) + \frac{1}{r}\frac{\partial}{\partial r}(r\rho v_r v_r) = -\frac{\partial p}{\partial r} + \frac{1}{r}\frac{\partial}{\partial r}\left[r\mu\left(2\frac{\partial v_r}{\partial r} - \frac{2}{3}(\nabla \cdot \mathbf{v})\right)\right] + \frac{1}{r}\frac{\partial}{\partial x}\left[r\mu\left(\frac{\partial v_x}{\partial r} + \frac{\partial v_r}{\partial x}\right)\right] - 2\mu\frac{v_r}{r^2} + \frac{2}{3}\frac{\mu}{r}(\nabla \cdot \mathbf{v}) \tag{3}$$

Energy equation:

$$\frac{\partial}{\partial t}(\rho E) + \nabla \cdot (\mathbf{v}(\rho E + p)) = -\nabla \cdot \left(\sum_j h_j J_j\right) + S_h \tag{4}$$

Species transport:

$$\frac{\partial}{\partial t}(\rho Y_i) + \nabla \cdot (\rho \mathbf{v} Y_i) = -\nabla \cdot \mathbf{J}_i + R_i + S_i \tag{5}$$

Turbulent flow is modeled in the context of Reynolds-averaged Navier–Stokes (RANS) and by using the realizable k–ε model [27]. Thermal radiation is further added to the computational model by applying discrete ordinates model, which is coupled with the energy equation, as discussed in Ref. [28]. The general

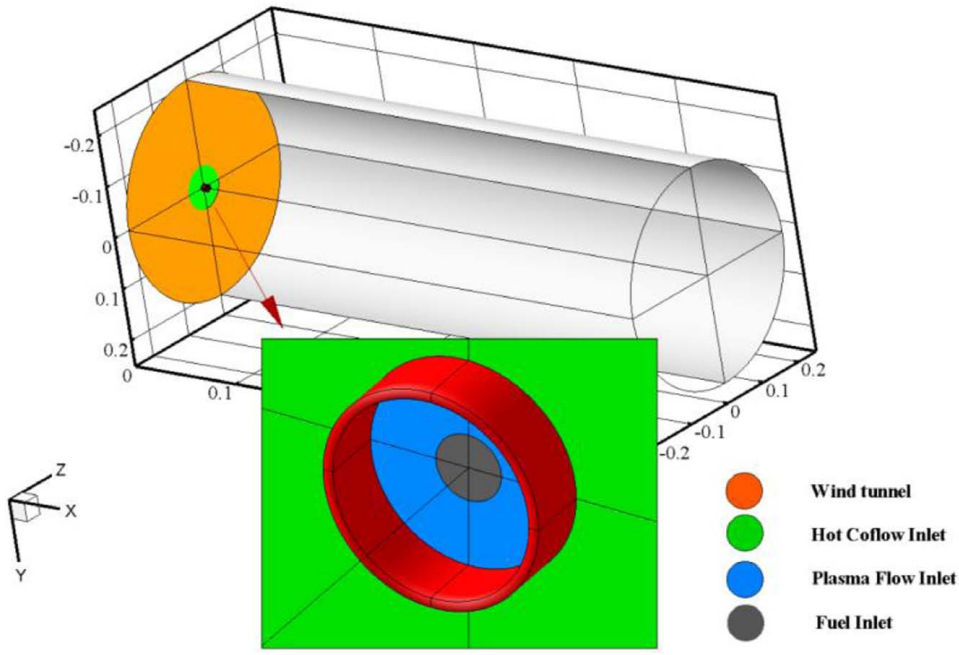

Fig. 1 Schematic of the burner with plasma actuator

conservation of chemical species is provided by Eq. (5) that solves for N-q species. The net source of chemical species I due to the reaction, R_i appearing as the source term in Eq. (5), is calculated as the sum of the reaction sources over the N_R reactions among the whole species. Turbulence-chemistry interactions are modeled by using the eddy dissipation concept (EDC). This is a well-established model applicable to a wide range of problems in turbulent combustion. In EDC method, the volume fraction of the fine structures (ξ^*) and the mean residence time (τ^*) are defined by the following relations

$$\xi^* = \left(\frac{3C_{D2}}{4C_{D1}}\right)\left(\frac{\nu\varepsilon}{k^2}\right)^{3/4} = C_\xi\left(\frac{\nu\varepsilon}{k^2}\right)^{3/4} \tag{6}$$

$$\tau^* = \left(\frac{C_{D2}}{3}\right)^{1/2}\left(\frac{\nu}{\varepsilon}\right)^{1/2} = C_\tau\left(\frac{\nu}{\varepsilon}\right)^{1/2} \tag{7}$$

Similar to the previous investigations [35], the volume fraction constant (C_ξ) and time scale constant (C_τ) are assumed to be 3 and 1, respectively. Equation (8) shows the mean reaction rate in the conservation equation, formulated for the mean species i is

$$R_i = \frac{\rho(\xi^*)^2}{\tau^*[1-(\xi^*)^3]}(Y_i^* - Y_i) \tag{8}$$

The eddy dissipation model allows for incorporation of extensive chemical mechanisms into turbulent reactive flows. In this study, GRI 2.11 reaction mechanism has been utilized. The reaction rate in this mechanism is given by the following relation

$$r = AT^b e^{-E_a/RT} \tag{9}$$

3 Plasma Injection Conditions

As expressed by Wada et al. [31], there are a large number of excited species which are produced by activating the dielectric barrier discharge (DBD) plasma actuator. The reaction mechanism below is a generally accepted mechanism to display the outlet species of 3%CH_4-97% air plasma actuator in the burner inlet [31,33,36]

$$\begin{aligned} &0.03CH_4 + 0.97(0.21O_2 + 0.79N_2) \rightarrow \\ &\quad aCH_4 + bO_2 + 0.7663N_2 + 0.00058CH_2O \\ &\quad + 0.00114H_2O + 0.000197H_2 + c(\text{7th species}) \end{aligned} \tag{10}$$

a, b, and c constants are related to seventh species which can be either of CO, CO_2, CH, CH_2, CH_3, C_2H_2, C_2H_4, and C_2H_6 species on the basis of the Lefkowitz's results [36]. Table 1 shows the constant coefficients of Eq. (10) based on the seventh species. Further, a number of studies have shown that about 50–80% of the plasma power is converted to thermal energy [37–42]. This implies that the outlet temperature of the plasma flow is between 470 K and 570 K [33].

Table 1 Constant coefficients of the Eq. (10) based on the seventh species

Case	Seventh species	a	b	c
1	CO	0.0290415	0.2026507	0.0003785
2	CO_2	0.0290415	0.2029745	0.1003785
3	CH	0.02891533	0.20284	0.0005046667
4	CH_2	0.028663	0.20284	0.000757
5	CH_3	0.027906	0.20284	0.001514
6	C_2H_2	0.0289153	0.20284	0.00025233
7	C_2H_4	0.02808334	0.20284	0.0006683318
8	C_2H_6	0.027906	0.20284	0.000757

Table 2 Operational conditions of the burner simulated in the present work [34]

Inlet condition	Composition, mass fraction	Axial velocity, m/s	Temperature, K
Fuel	$H_2 = 11.1$, $CH_4 = 88.9$	70	300
Co-flow	$O_2 = 3$, $N_2 = 88$, $H_2O = 6.5$, $CO_2 = 5.5$	3.2	1300
Wind tunnel	$O_2 = 23.3$, $N_2 = 76.7$	3.2	300

4 Flow Configuration, Grid Independency, and Validation

Figure 1 shows the schematic view of the burner that was computationally modeled in this work. The basis of this burner was developed by Dally et al. [34] and Christo and Dally [43]. It includes three parts of fuel inlet, hot co-flow inlet, wind tunnel, and the boundary condition in case of without plasma injection (traditional MILD combustion (TMC)), as shown in Table 2. In the original Dally's burner, the flows of fuel and gases are injected to the burner axially. The burner includes a wind tunnel, hot co-flow inlet and fuel inlet with diameters of 210, 80, and 4.25 mm, respectively. The air entering the wind tunnel consists of 23% O_2 and 77% N_2 with the velocity of 3.2 m/s. Temperature of the wind tunnel is kept constant at 300 K and the hot co-flow is preheated up to 1300 K. The hot co-flow includes N_2, H_2O, CO_2, and O_2 and features a velocity of 3.2 m/s in the case of TMC. Also, the fuel injected at the center of the burner is a blend of H_2-CH_4 (11.1%, 88.9%) with the Reynolds number of 10,000.

In the current investigation, an annular nozzle (see Fig. 1) is added in order to inject the plasma flow based on the conditions of Wada et al. [31] studies. The temperature of plasma flow is 570 K [33], and at the inlet, the velocity of this flow is the same as the hot co-flow. The DBD is generated between two coaxial electrodes of which the outer one (i.e., conical copper electrode) is covered with a dielectric material made of quartz. The center burner's wall acts as a positive electrode of the DBD actuator used in the plasma reactor, and the plasma discharge occurs in the regions close to the exit of the quartz tube. The dielectric barrier is elongated 4.25 mm past the tip of the jet exit to avoid the formation of arc discharge over its lips. Thermally insulated center burner and plasma reactor section are considered. Figure 2 shows the grid

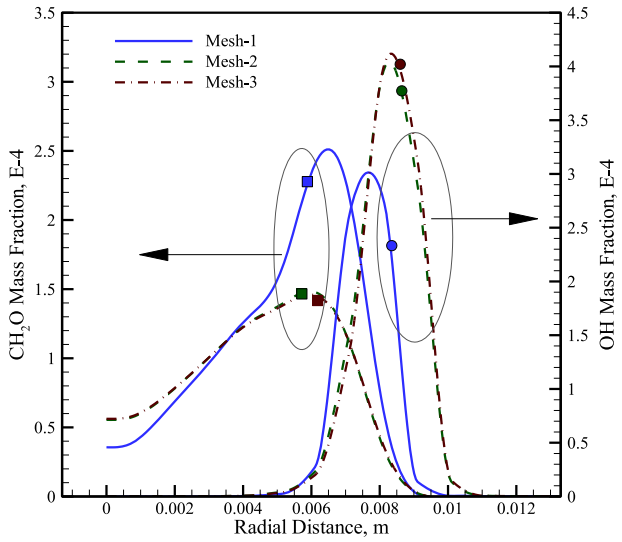

Fig. 2 Mesh independency study

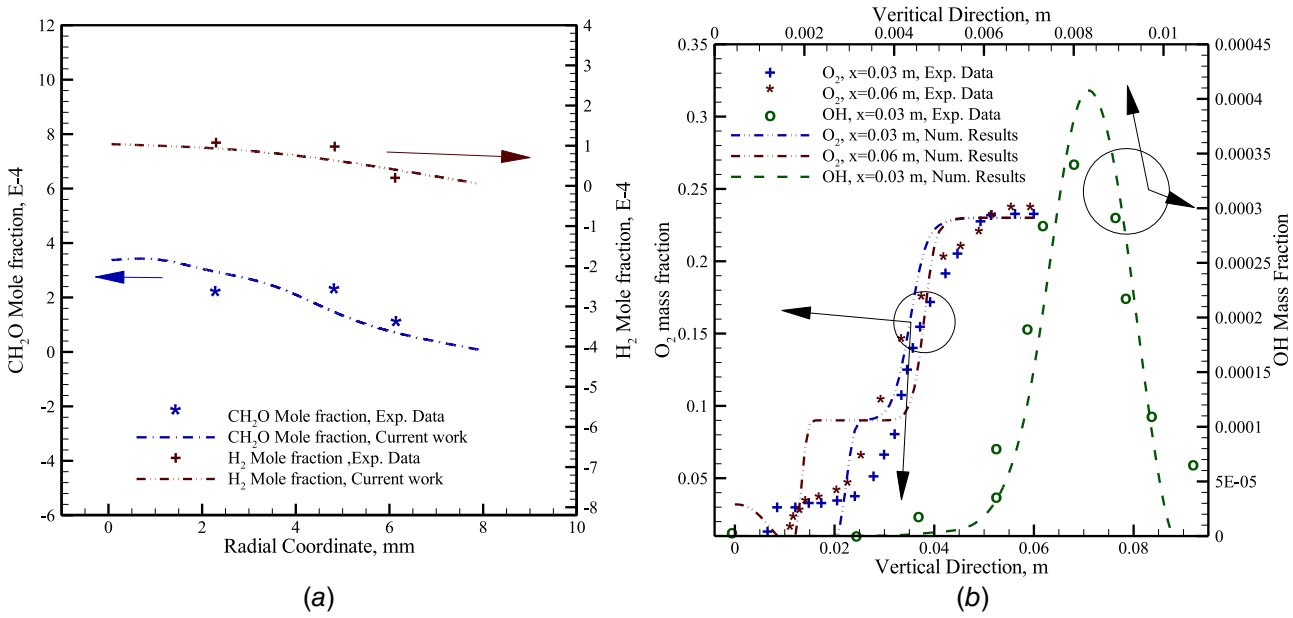

Fig. 3 Comparison between the present numerical results and the experimental data of (*a*) Adapted from Ref. [35] and (*b*) Adapted from Ref. [34]

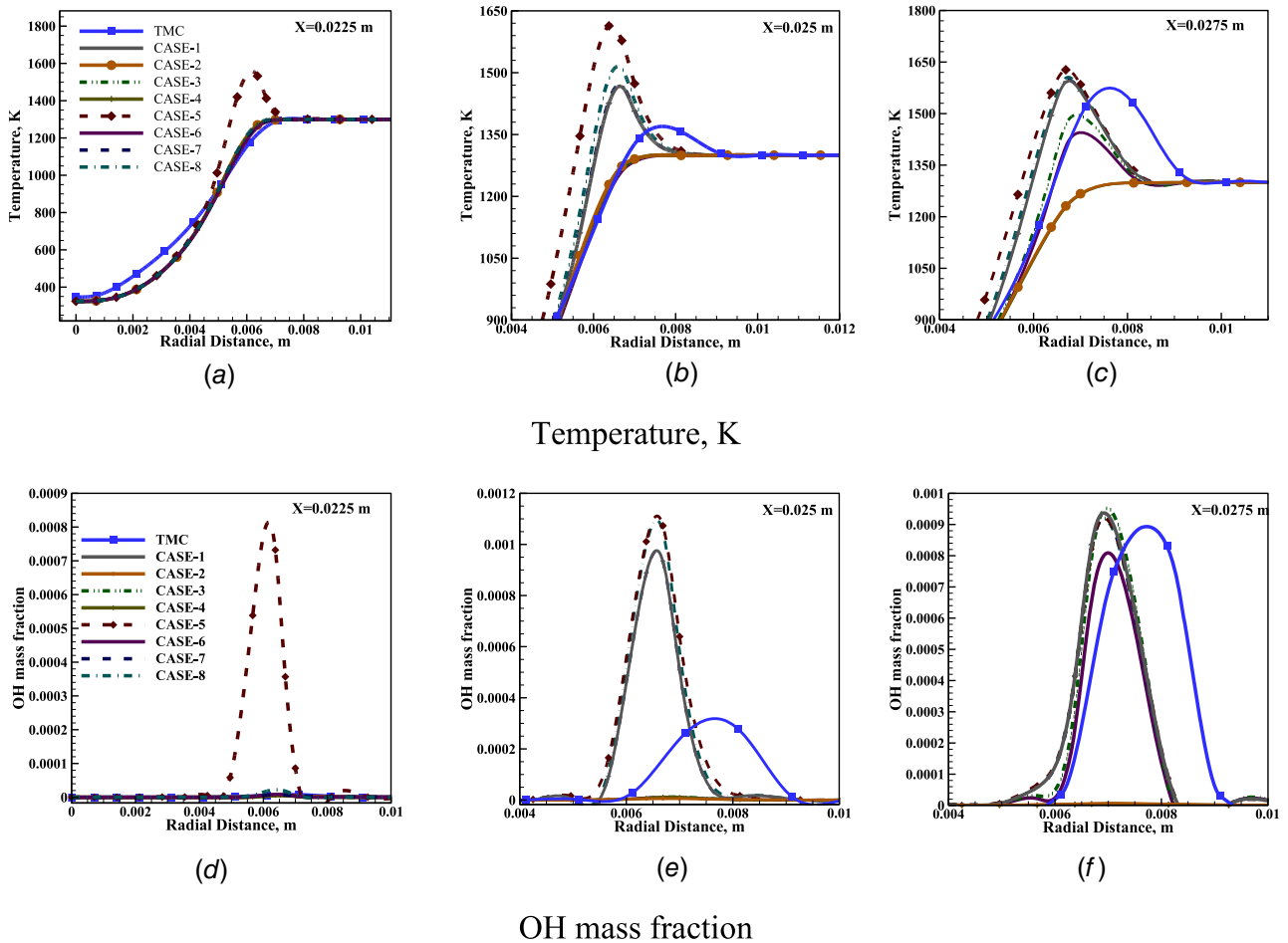

Fig. 4 Radial temperature and mass fraction of OH radical distributions at different axial locations measured from the inlet nozzle. Cases 1–8 are defined in Table 1.

sensitivity analysis of the current work. To evaluate the level of grid independency of the results, three mesh structures consisting of 23,000 cells (mesh 1), 45,000 cells (mesh 2), and 80,000 cells (mesh 3) were used. Figure 2 indicates the outcomes for the mass fractions of CH_2O and OH radicals. Evidently, the results of the computational mesh with more than 45,000 cells are independent of the cell size. Hence, this grid is used for the rest of investigations reported in this paper.

To ensure the validity of the numerical analysis, the simulation results are compared with the experimental data extracted from the literature. First, the numerical results are compared with the experimental data [31] for H_2 and CH_2O mole fractions in a plasma-assisted MILD combustion burner (see Fig. 3(*a*)). Evidently, the present approach is suitable to predict the effects of plasma actuator on combustion behavior. Figure 3(*b*) shows a comparison between the current numerical results and the experimental data of Dally et al. [34] for O_2 mass fraction in the axial locations of 0.03 m and 0.06 m as well as OH mass fraction at the axial distance of 0.03 m from the injection point. As depicted by this figure, the utilized finite volume solver can predict the behaviors of MILD combustion with good accuracy.

5 Results and Discussion

5.1 General Behavior of the Reacting Flow. In this section, the effects of plasma flow injection on MILD combustion behavior are investigated. The inlet component of the plasma flow to the burner is based on the right-hand side of Eq. (10) and the constant coefficients of Table 1. Figures 4(*a*)–4(*f*) show the radial temperature and OH mass fraction distribution for different cases in the axial distances of 0.0225, 0.025, 0.0275, and 0.03 m from the inlet nozzle. Each of the eight cases analyzed in this figure refer to the release of one of the species listed in Eq. (10). At 0.0225 m away from the inlet nozzle, there is a temperature jump for case 5 implying that combustion occurs only when CH_3 is released from the plasma nozzle. All other investigated cases and the conventional TMC do not feature any reaction. In the axial distance of 0.025 m (Fig. 4(*b*)), temperature jumps are observed for cases 1, 5, 8, and TMC. The extent of these jumps varies significantly among the species and clearly the smallest temperature overshoot corresponds to TMC or no plasma case. Among the plasma cases, injection of CH_3 results in the maximum temperature jump (around 400 K), indicating that this is the most influential species in intensifying

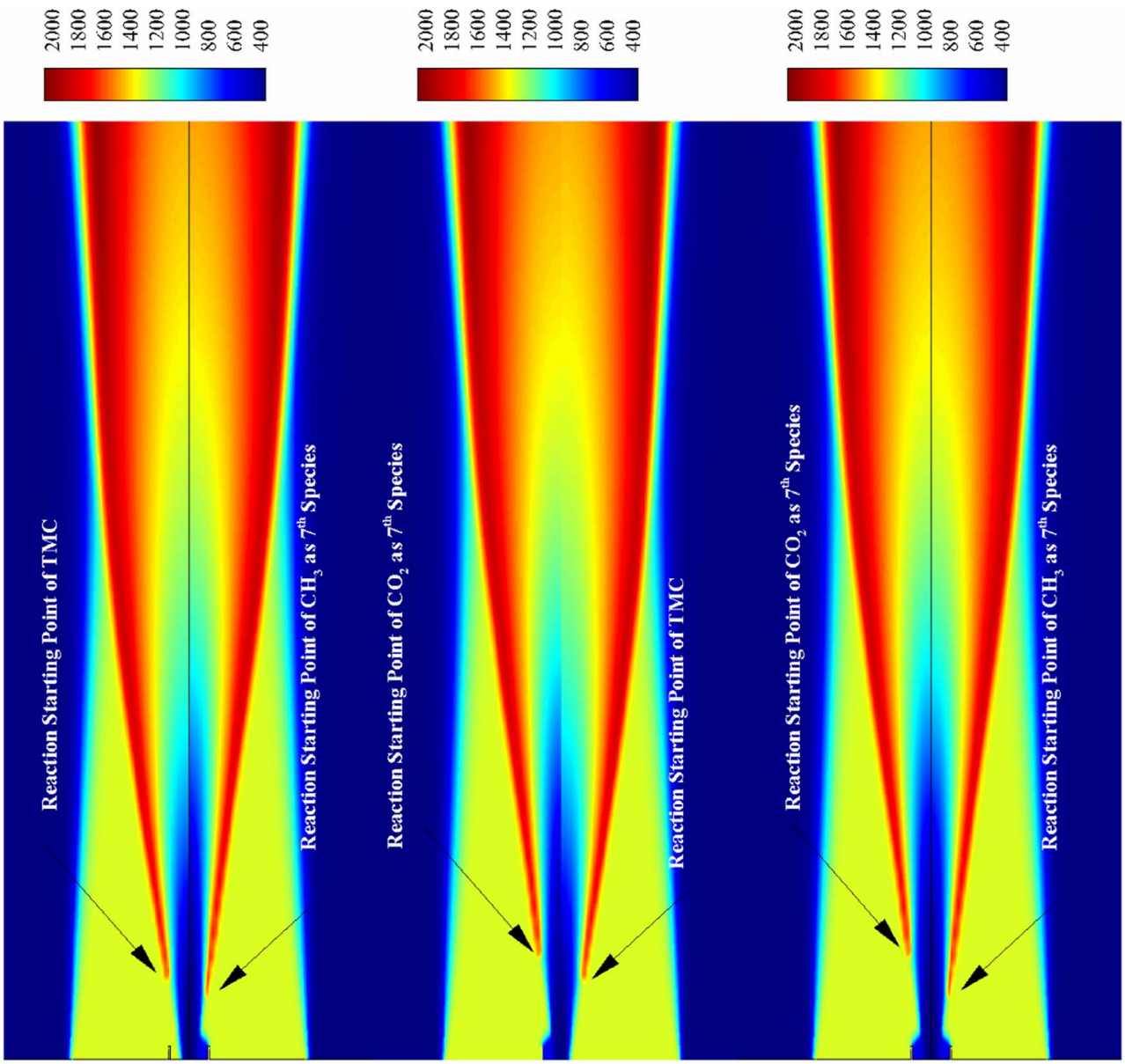

Fig. 5 Contours of temperature for TMC, and release of CH_3 (case 5) and CO_2 (case 2)

Table 3 Reaction starting point for different seventh species

Seventh species	CO	CO_2	CH	CH_2	CH_3	C_2H_2	C_2H_4	C_2H_6
Axial distance of onset of reaction zone, m	0.02381	0.03847	0.02607	0.031	0.01957	0.026073	0.02444	0.02363

the combustion process [33]. At the axial location of 0.0275 m, the temperature effects of addition of C_2H_4, C_2H_2, CH, CH_2, and CO_2, are more and less similar to those of TMC (see Fig. 4(*c*)). Yet, this is clearly not the case for CO_2 and CH_2, as they act as inhibitors and delay combustion to the axial distance of 0.03 m.

These findings are further elaborated in Fig. 5 which shows the contours of temperature for TMC case, case 2, and case 5. A comparison between the temperature distribution of TMC and MILD combustion with plasma injection reveals that the reaction lift-off for case 5 (plasma flow with CH_3 species) is smaller than that of TMC. Also, the lift-off in TMC case is smaller than that when CO_2 is injected. These confirm the findings of Figs. 4(*a*)–4(*c*) and demonstrate the intensifying and inhibitory effects of adding CH_3 and CO_2. Figures 4(*d*)–4(*f*) illustrate the radial distribution of OH radical, a major factor indicating the heat release of a combustion process, for different cases listed in Table 1. An increase in temperature increases the OH concentration and given the earlier discussion, it is anticipated that the OH value to be highest for case 5. In keeping with this, Figs. 4(*d*)–4(*f*) show that for all axial locations the amount of OH radical is at its highest value for case 5. Also, the OH species represents the region in which the chemical reaction takes place [44] and it is clear that by injecting the plasma flow the reaction region shrunk. The decrease in radial extent of the reactive region might be due to the presence of electrodes in the plasma actuator that prevents the reactive zone to spread at the burner inlet. A comparison among the different cases reveals that the heat release for case 5, especially in the input region, is higher than that for the other cases. In addition, considering the distribution of OH radical reveals that no chemical reaction has taken place for cases 2 and 4 before reaching the axial location of 0.03 m, as the OH concentration is zero. The location of reaction zone can be indicated by the change in concentration of OH radical [44]. As clearly demonstrated by Table 3, the lift-off value for case 5 is the lowest in comparison with all other cases.

The graphs in Figs. 6(*a*)–6(*d*) represent the radial distribution of the mass fraction of HCO (formyl) radical, which represents the rate of heat release [45]. It is observed that at the axial distance of 0.02 m from the inlet nozzle the HCO radical mass fraction for the TMC mode is higher than the other cases. By moving slightly away from the inlet region, the mass fraction of formyl radical becomes almost twice as that at $x = 0.02$ m. Yet, the increase in the concentration of HCO for case 2 is much stronger and shows a growth of nearly eight times in between $x = 0.02$ m and $x = 0.0225$ m. Figures 6(*a*)–6(*d*) show that for cases with plasma injection the concentration of HCO radical constantly increases along the centerline, while this growth is much less noticeable for TMC. At the distance of 0.03 m, the mass fraction of CHO for TMC is a few orders of magnitude smaller than that of all other plasma generated species (with exception of CO_2 and CH_2). In addition, Figs. 6(*e*) and 6(*f*) depict the radial distribution of the rates of thermal and prompt NO formation for cases 1–8 and TMC. Figure 6(*e*) shows that for most cases, although shifted radially, the radial distribution of prompt NO is mostly similar among the investigated cases. Exceptions to this are cases 4, 5, and 7. In particular, case 5 has a noticeably higher rate of prompt NO formation in comparison with the rest of the investigated cases. Comparing to prompt NO, the variations in

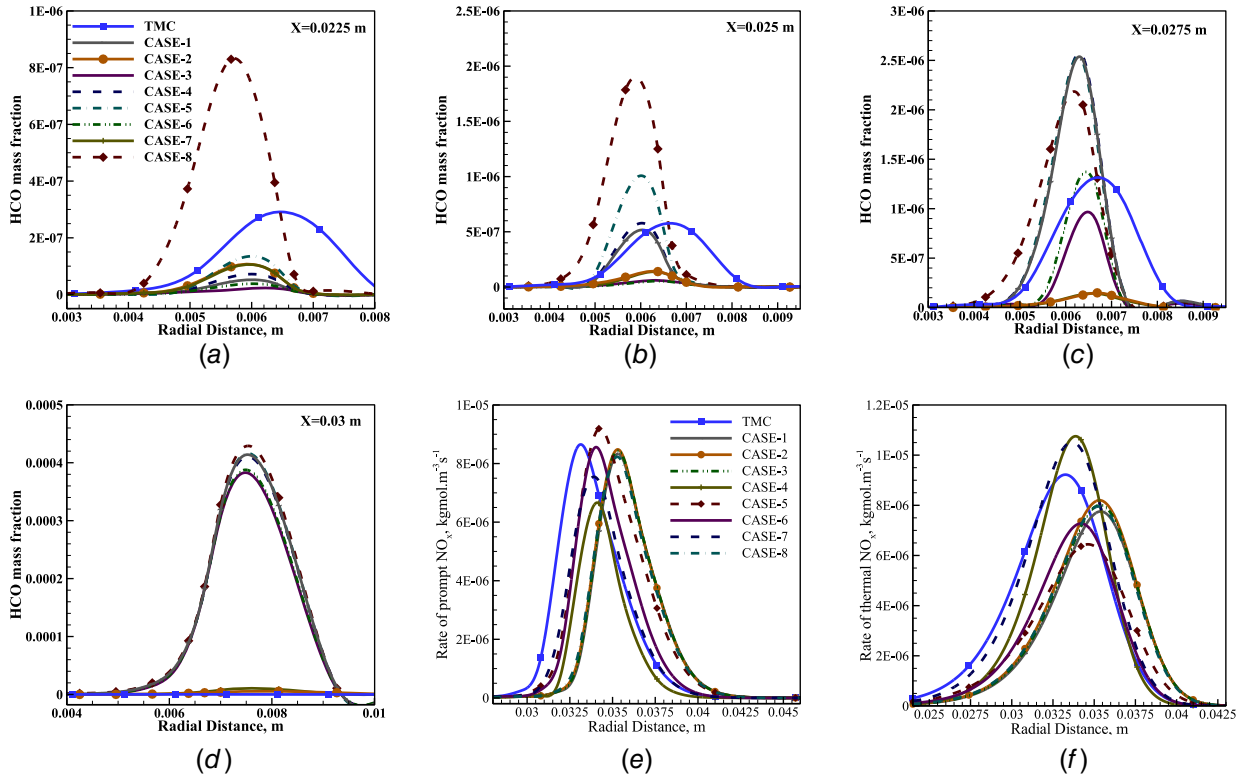

Fig. 6 (*a–d*) Radial distribution of the mass fraction of HCO at different axial locations, (e) prompt NO, and (*f*) thermal NO formation

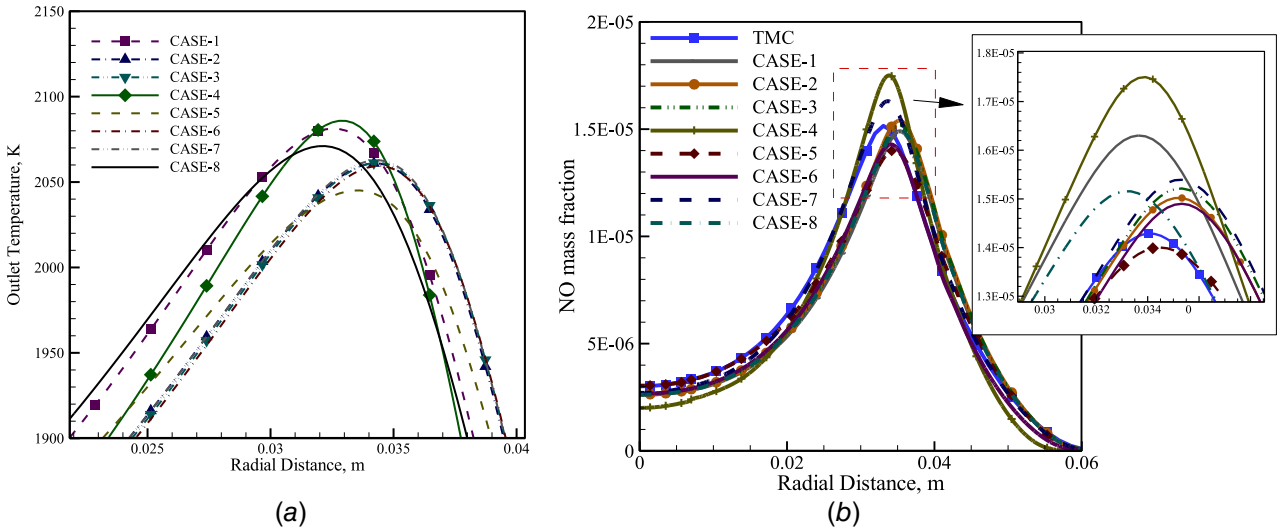

Fig. 7 (*a*) Burner outlet temperature for different cases and (*b*) radial distribution of the mass fraction of NO at the burner outlet

thermal NO formation are more significant (see Fig. 6(*f*)). This is related to the influences of plasma injection upon the flow temperature which will be further discussed later. Nonetheless, it is interesting to note that the thermal NO is the lowest for case 5. Although not shown in here, an essential species affecting the formation of prompt NO is hydroperoxyl radical (HO_2) [46,47].

According to Fig. 7(*a*), which represents the outlet temperature of the burner, the outlet flow temperature for case 5 has the lowest value among all simulated cases. It follows that based on Zeldovich's mechanism of NO formation; the thermal NO is reduced in this case. In general, for methane combustion, prompt NO contribution to the total NO emissions, is much smaller than that of thermal NO. This explains why in Fig. 7(*b*) case 5 features the lowest total NO emission among all the simulated cases.

5.2 Effects of Inlet Reynolds Number and Plasma Temperature. In the previous section, it was found that case 5 (injection of CH_3) leads to a more complete combustion. In this section, we investigate the effects of changes in Reynolds number and inlet temperature of the plasma flow upon the behaviors of MILD combustion. For this purpose, the conditions in Table 4 are considered. Figure 8 shows the radial temperature distributions for the axial distances of 0.1, 0.15, 0.25, and 0.45 m from the inlet nozzles. It is observed that the changes in Reynolds number of the inlet plasma flow cause considerable variations in the temperature distributions at different axial locations. At low Reynolds numbers and for axial locations close to the inlet, the combustion temperature is lower than that for higher Reynolds numbers. This is because reduction of Reynolds number increases the residence time of the mixture and leads to a more stable reacting flow, which could then cause an increase in the combustion temperature. It helps the inlet fuel to be burnt at a shorter distance to the inlet nozzle and, as shown by Fig. 9, at lower Reynolds numbers the amount of unburned fuel declines. This is further confirmed by Table 5, which shows the starting point of reaction zone along the burner centerline. It is clear that this point moves closer to the inlet nozzle by reduction of the Reynolds number of the inlet plasma flow. This trend implies that the ignition delay is reduced by decreasing the inlet Reynolds number of the plasma flow. By decreasing the ignition delay and increasing the residence time, it is expected that the combustion temperature increases gradually. Referring to Fig. 8, it is observed that at the axial distance of 0.45 m (near the burner outlet) the maximum flow temperature occurs at the lowest Reynolds number of the plasma flow. At locations closer to the inlet crater (axial distances of 0.1 m and 0.15 m), the combustion temperature is higher for the higher Reynolds numbers. This is due to the enhanced turbulence intensity of the reacting flow with increasing Reynolds number, which then renders a more complete combustion.

Table 4 Value of Reynolds number for inlet plasma flow

Case	R1	R2	R3	R4
Inlet plasma flow Reynolds number	1000	4000	6000	8000

As shown in Fig. 9, the amount of unburned fuel has decreased by moving away from the inlet zone. This amount is more for higher Reynolds number in the axial distances of 0.1 and 0.15 m. However, the amount of unburned fuel for case of R4 is lower than that for R1 case. Therefore, taking into account Figs. 8 and 9 that represent the temperature and unburned fuel distribution, respectively, the following argument can be made. As the Reynolds number of the plasma flow increases, the centerline temperature initially decreases due to getting away from the adiabatic flame temperature and after that it increases gradually by moving away from the entrance zone.

Figure 10(*a*) shows the distribution of OH radical for different Reynolds numbers of the plasma flow and at different axial locations. This figure implies that as the Reynolds number of plasma flow increases, the volume and width of the flame decrease. However, the amount of OH radical has increased by augmenting the Reynold number of plasma flow and, as a result the heat release has increased. Further, Fig. 10(*b*) depicts the radial distribution of the molar concentration of formyl radical (HCO) at different axial locations. HCO is an essential intermediate species in the combustion of hydrocarbon [48]. In hydrocarbon flames, HCO radical is generated by abstraction of a hydrogen atom from formaldehyde produced through the reaction of methyl radicals with atomic oxygen. The chain branching rate is determined by the competition between thermal decomposition of formyl radical (HCO → H + CO) and the bimolecular reactions of the radical. The process affects several key combustion characteristics including autoignition thresholds and delays as well as the flame propagation speed [49,50].

Figure 10(*b*) indicates that the amount of formyl radical increases with increasing the Reynolds number of the inlet plasma flow. According to this figure, the radial distribution of formyl radical, representing the heat release [51], is highly dependent on the Reynolds number of the plasma flow entering the reactive region. It is, therefore, evident that the amount of HCO at low Reynolds

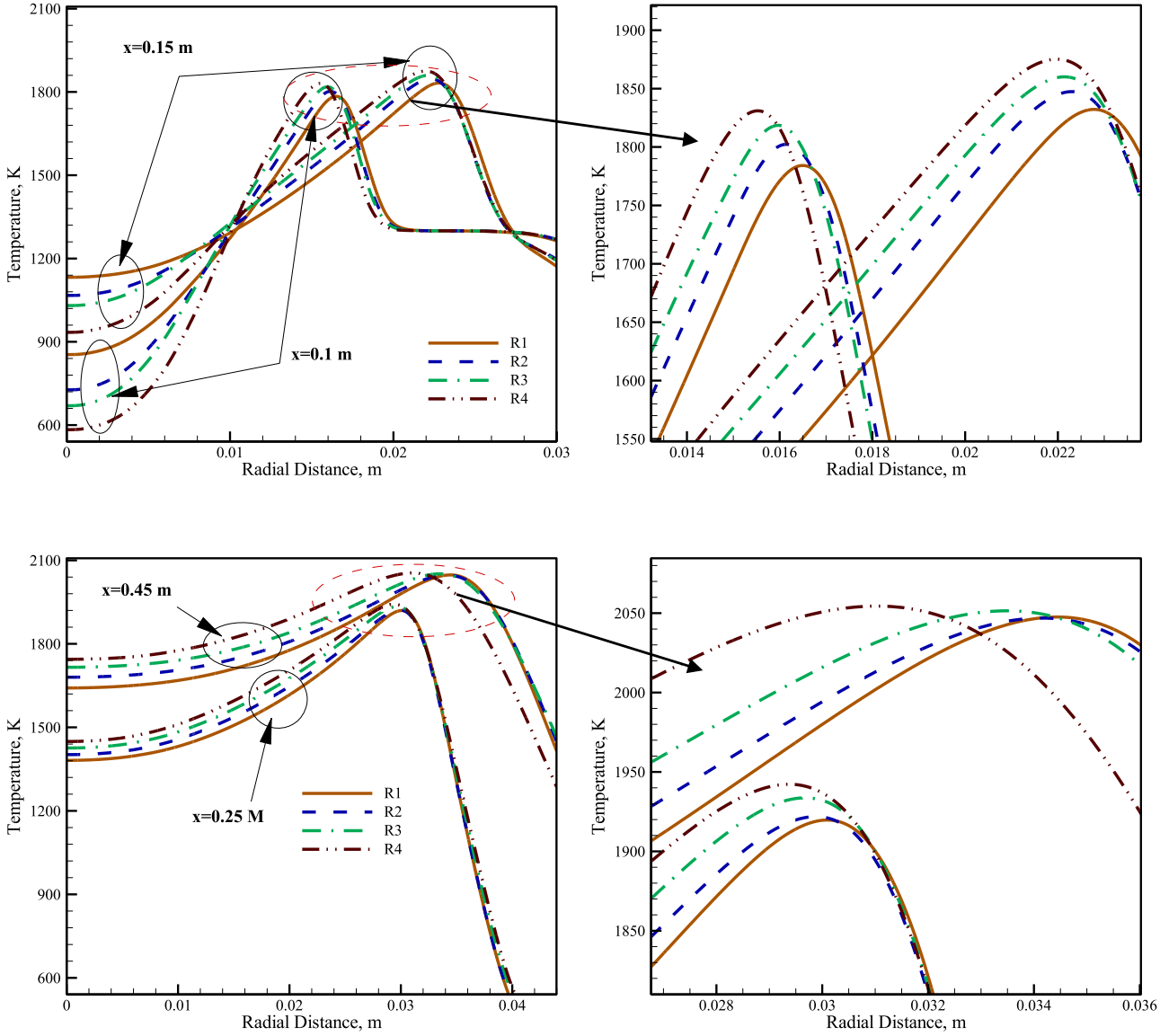

Fig. 8 Radial distribution of the flow temperature at different axial locations

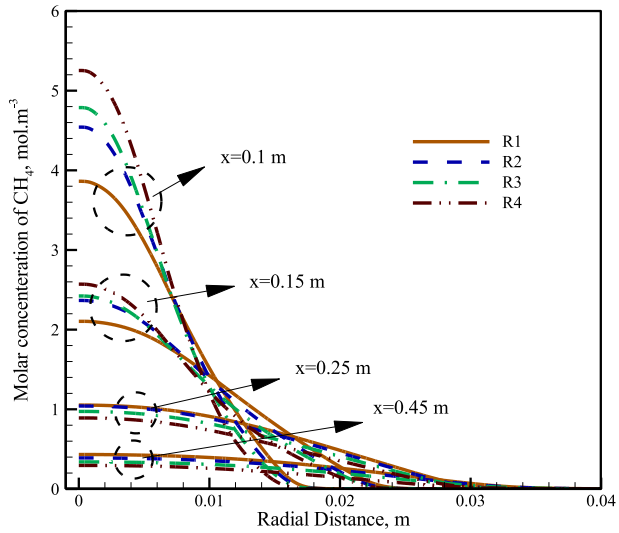

Fig. 9 Radial distribution of molar concentration of CH_4 at different axial locations and for various Reynolds numbers of the plasma flow

numbers is significantly lower than that at higher Reynolds number of the inlet plasma flow. Hence, in comparison with the higher Reynolds number cases, the heat release is lower. Furthermore, according to Fig. 10(*c*), the production rate of thermal NO correlates with the Reynolds number of the plasma flow. Figure 8 already showed that the maximum combustion temperature increases at higher values of Reynolds number of the plasma flow. Since there is a direct relation between thermal NO emissions and temperature, the use of high Reynolds number for plasma flow leads to an increase in the thermal NO emission as shown in Fig. 10(*c*). Further, due to decrease in the residence time at higher Reynolds numbers, the prompt NO increase. Hence, based on Fig. 10(*c*),

Table 5 The axial distance of onset of the reaction zone from the nozzle inlet for various Reynolds numbers of the plasma flow

Case	R1	R2	R3	R4
Axial distance of onset of the reaction zone from the nozzle inlet, m	0.029969	0.038414	0.044893	0.064923

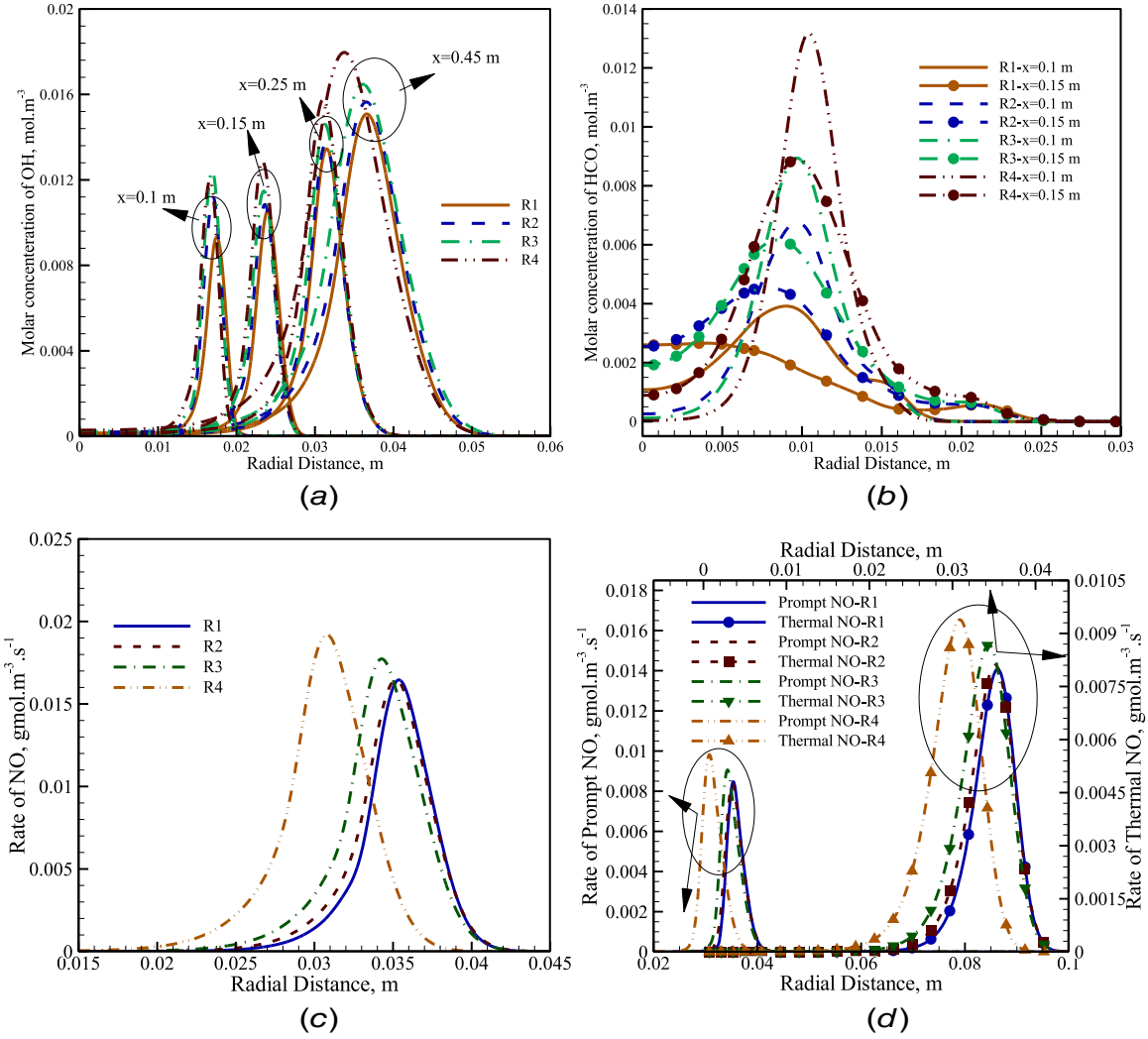

Fig. 10 Molar concentration of OH and HCO, and the rate of prompt and thermal NO and outlet NO at various Reynolds numbers of the plasma flow

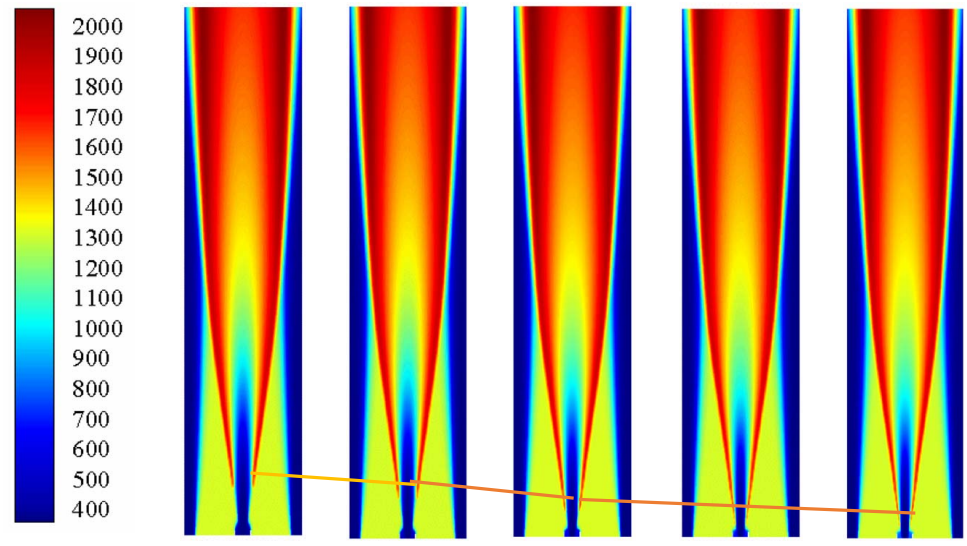

Fig. 11 Temperature distribution and reaction starting point for various plasma temperatures

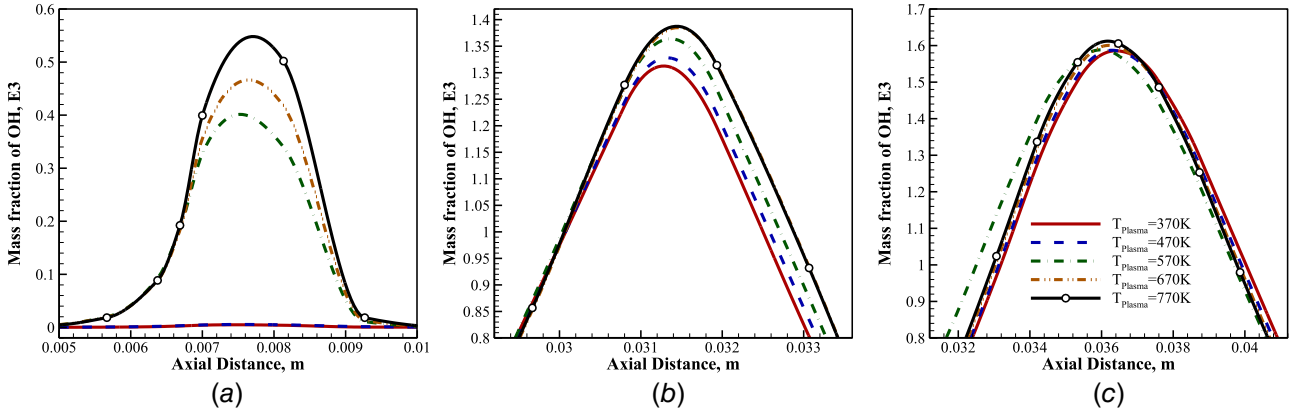

Fig. 12 Mass fraction of OH radical for various plasma temperatures at (*a*) x = 0.03 m, (*b*) 0.25 m, and (*c*) 0.45 m

the rate of prompt NO increases with increasing the inlet Reynolds number of the plasma flow. This is depicted by Fig. 10(*d*) which shows the rate of NO emission at the outlet zone of the burner. Clearly, increases in the Reynolds number of the plasma flow magnify the amount of NO rather significantly. As a remedy, the preheating temperature of co-flow can be reduced to prevent occurrence of high temperatures in the reactive flow and thus suppress the mechanism of thermal NO. By doing this, the conditions of MILD combustion are retained, and the NO emissions are reduced.

Next, the influences of temperature variations in plasma flow, with CH_3 as the seventh specifies (in Eq. (10)), upon the behavior of MILD combustion are investigated. To this end, the plasma flow temperature is set at 370, 470, 570, 670, and 770 K. Figure 11 shows the spatial temperature distribution of the reacting flow and the starting point of the reaction for different plasma flow temperatures. As the inlet flow temperature increases, the reactive flow tends to react more quickly. Consequently, as depicted by Fig. 11, the temperature rise point moves toward the inlet nozzle as the plasma flow temperature increases. This means that the ignition delay is reduced and therefore it increases residence time of the reacting flow. Furthermore, applying higher values of plasma flow temperature cause the combustible flow to mix in shorter times which in turn leads to the increase in heat release. This is confirmed by Fig. 12 which shows that the amount of OH mass fraction increases with augmenting the temperature of plasma flow. By moving away from the inlet ($x = 0.25$ m), the OH radical is equilibrated for temperatures of 670 K and 770 K. This indicates a reduction in the effects of plasma flow temperature by moving away from the entrance area. Besides, in the zone near the burner outlet ($x = 0.45$ m), the OH radical is almost equal for all plasma flow temperatures. It is, nonetheless, important to note that the increase in inlet plasma temperature does not change the flame width significantly.

6 Conclusions

The effects of applying a nonequilibrium plasma discharge upon the performance of a conventional MILD combustor fueled by a mixture of methane and hydrogen was investigated numerically. A wide range of species including C_2H_2, C_2H_4, C_2H_6, CH, CH_2, CH_3, CO, and CO_2 were injected by a plasma torch into an otherwise TMC burner. The turbulent reactive flow was modeled through taking a RANS approach coupled with detailed chemical kinetics (GRI. 2.11). The results showed that CH_3 is the most effective species to improve MILD combustion. The other key findings of this study can be summarized as follows:

- Injection of CH_3 as plasma results in the reduction of the ignition delay and NO emission. It also leads to enhancement of the amount of OH radical and heat release. Further, a comparison between the temperature distribution of TMC and MILD combustion with plasma injection reveals that the reaction lift-off for plasma flow with CH_3 species is smaller than that of TMC. Furthermore, with the injection of plasma containing CH_3 radical, a region with high concentration of formaldehyde is developed close to the plasma nozzle.
- At low Reynolds numbers of the plasma flow and for the axial locations close to the inlet, the combustion temperature is lower than that at higher Reynolds numbers. By increasing the plasma temperature, starting point of the reaction zone along the burner centerline moves closer toward the inlet nozzle.
- Near the burner outlet, the maximum flow temperature occurs at the lowest Reynolds number of the plasma flow. At locations closer to the inlet nozzle, the combustion temperature is higher for the higher Reynolds numbers.
- As the Reynolds number of the plasma flow increases, the centerline temperature initially decreases and then increases gradually by moving away from the entrance zone.
- The amount of OH radical increases by augmenting the Reynold number of plasma flow and, as a result the process heat release increases. Further, the amount of formyl radical increases at higher Reynolds numbers of the inlet plasma flow.
- The application of high Reynolds number for plasma flow leads to an increase in the thermal and prompt NO emission.
- Applying higher values of plasma flow temperature causes the combustible flow to mix in shorter times which in turn leads to higher rates of heat release.

Acknowledgment

N. Karimi acknowledges the financial support of Engineering and Physical Science Research Council through Grant EP/N020472/1.

Data Availability Statement

The authors attest that all data for this study are included in the paper. Data provided by a third party listed in Acknowledgment. No data, models, or code were generated or used for this paper.

Nomenclature

h = enthalpy
k = turbulence kinetic energy
p = pressure
r = radial direction
A = pre-exponential factor
E = energy
N = total number of fluid phase chemical species present in the system

R = gas constant
T = temperature, K
Z = mixture fraction
v_r = radial velocity
v_x = x-velocity
C_ξ = volume fraction constant
C_τ = time scale constant
E_a = activation energy
J_i = diffusion flux of species i
R_i = net rate of production of species i by chemical reaction
S_h = heat of chemical reaction, and any other volumetric heat sources
S_i = rate of creation by addition from the dispersed phase plus any user-defined sources
W_j = atomic mass for element j
Y_i^* = fine-scale species mass fraction after reacting over the time τ^*

Greek Symbols

ε = rate of dissipation of turbulence energy
μ_i = eddy viscosity, Pa·s
ν = kinematic viscosity, m^2/s
ξ^* = length fraction of the fine scales
ρ = density, kg/m^3

References

[1] Said, A. O., and Gupta, A. K., 2015, "Oxygen Enriched Air Effects on Combustion, Emission, and Distributed Reaction," ASME J. Energy Resour. Technol., **137**(4), p. 042203.
[2] Wang, L., Karimi, N., Sutardi, T., and Paul, M. C., 2019, "Combustion Characteristics and Pollutant Emissions in Transient Oxy-Combustion of a Single Biomass Particle: A Numerical Study," Energy Fuels, **33**(2), pp. 1556–1569.
[3] Cavaliere, A., and de Joannon, M., 2004, "Mild Combustion," Prog. Energy Combust. Sci., **30**(4), pp. 329–366.
[4] Moghadasi, M. H., Riazi, R., Tabejamaat, S., and Mardani, A., 2019, "Effects of Preheating and CO_2 Dilution on Oxy-MILD Combustion of Natural Gas," ASME J. Energy Resour. Technol., **141**(12), p. 122002.
[5] Liu, R., and An, E., 2017, "Turbulent Flame Characteristics of Oxycoal MILD Combustion," ASME J. Energy Resour. Technol., **139**(6), p. 062206.
[6] Wang, L., Karimi, N., and Paul, M. C., 2018, "Gas-Phase Transport and Entropy Generation During Transient Combustion of Single Biomass Particle in Varying Oxygen and Nitrogen Atmospheres," Int. J. Hydrogen Energy, **43**(17), pp. 8506–8523.
[7] Hosseinalipour, S. M., Fattahi, A., and Karimi, N., 2016, "Investigation of the Transmitted Noise of a Combustor Exit Nozzle Caused by Burned Hydrogen-Hydrocarbon Gases," Int. J. Hydrogen Energy, **41**(3), pp. 2075–2086.
[8] Mousavi, S. M., Abolfazli Esfahani, J., and Jafari, D., 2012, "The Effect of Adding H_2 to the Flameless Oxidation (FLOX) of Biogas on Pollutants Emission," 2nd Annual Clean Energy Conference (ACEC), Cilivica, Kerman, Iran.
[9] Hunt, G., Torabi, M., Govone, L., Karimi, N., and Mehdizadeh, A., 2018, "Two-Dimensional Heat and Mass Transfer and Thermodynamic Analyses of Porous Microreactors With Soret and Thermal Radiation Effects—An Analytical Approach," Chem. Eng. Process., **126**, pp. 190–205.
[10] Christodoulou, L., Karimi, N., Cammarano, A., Paul, M., and Navarro-Martinez, S., 2020, "State Prediction of an Entropy Wave Advecting Through a Turbulent Channel Flow," J. Fluid Mech., **882**, p. A8.
[11] Chinnici, A., Nathan, G. J., and Dally, B. B., 2018, "Combined Solar Energy and Combustion of Hydrogen-Based Fuels Under MILD Conditions," Int. J. Hydrogen Energy, **43**(43), pp. 20086–20100.
[12] Chinnici, A., Tian, Z. F., Lim, J. H., Nathan, G. J., and Dally, B. B., 2019, "Thermal Performance Analysis of a Syngas-Fuelled Hybrid Solar Receiver Combustor Operated in the MILD Combustion Regime," Combust. Sci. Technol., **191**(1), pp. 2–17.
[13] Chinnici, A., Nathan, G. J., and Dally, B. B., 2019, "An Experimental Study of the Stability and Performance Characteristics of a Hybrid Solar Receiver Combustor Operated in the MILD Combustion Regime," Proc. Combust. Inst., **37**(4), pp. 5687–5695.
[14] Xie, Y., Tu, Y., Jin, H., Luan, C., Wang, Z., and Liu, H., 2019, "Numerical Study on a Novel Burner Designed to Improve MILD Combustion Behaviors at the Oxygen Enriched Condition," Appl. Therm. Eng., **152**, pp. 686–696.
[15] Mousavi, S. M., Kamali, R., Sotoudeh, F., Karimi, N., and Jeung, I.-S., 2020, "Numerical Investigation of the Effects of Swirling Hot Co-Flow on MILD Combustion of a Hydrogen–Methane Blend," ASME J. Energy Resour. Technol., **142**(11), p. 112301.
[16] Mousavi, S. M., and Abolfazli-Esfahani, J., 2014, "Numerical Investigation of the Flameless Oxidation of Natural Gas in the IFRF Furnace Using Large Eddy Simulation," Int. J. Spray Combust. Dyn., **6**(4), pp. 387–410.
[17] Mousavi, S. M., 2014, "Numerical Study of Entropy Generation in the Flameless Oxidation Using Large Eddy Simulation Model and OpenFOAM Software," Int. J. Thermodyn., **17**(4), pp. 202–208.
[18] Kamali, R., Mousavi, S. M., Binesh, A. R., and Abolfazli-Esfahani, J., 2016, "Large Eddy Simulation of the Flameless Oxidation in the IFRF Furnace With Varying Inlet Conditions," Int. J. Spray Combust. Dyn., **9**(2), pp. 102–115.
[19] Deng, X., Xiong, Y., Yin, H., and Gao, Q., 2016, "Numerical Study of the Effect of Nozzle Configurations on Characteristics of MILD Combustion for Gas Turbine Application," ASME J. Energy Resour. Technol., **138**(4), p. 042212.
[20] Starik, A., Loukhovitski, B., Sharipov, A., and Titova, N., 2015, "Physics and Chemistry of the Influence of Excited Molecules on Combustion Enhancement," Philos. Trans. R. Soc., A, **373**(2048), p. 20140341.
[21] Li, P., Mi, J., Dally, B. B., Craig, R. A., and Wang, F., 2011, "Premixed Moderate or Intense Low-Oxygen Dilution (MILD) Combustion From a Single Jet Burner in a Laboratory-Scale Furnace," Energy Fuels, **25**(7), pp. 2782–2793.
[22] Pilla, G., Galley, D., Lacoste, D. A., Lacas, F., Veynante, D., and Laux, C. O., 2006, "Stabilization of a Turbulent Premixed Flame Using a Nanosecond Repetitively Pulsed Plasma," IEEE Trans. Plasma Sci., **34**(6), pp. 2471–2477.
[23] Kim, W., Mungal, M. G., and Cappelli, M. A., 2008, "Formation and Role of Cool Flames in Plasma-Assisted Premixed Combustion," Appl. Phys. Lett., **92**(5), p. 051503.
[24] Sun, W., Won, S. H., Ombrello, T., Carter, C., and Ju, Y., 2013, "Direct Ignition and S-Curve Transition by In Situ Nano-Second Pulsed Discharge in Methane/Oxygen/Helium Counterflow Flame," Proc. Combust. Inst., **34**(1), pp. 847–855.
[25] Sun, W., Won, S. H., and Ju, Y., 2014, "In Situ Plasma Activated Low Temperature Chemistry and the S-Curve Transition in DME/Oxygen/Helium Mixture," Combust. Flame, **161**(8), pp. 2054–2063.
[26] Yin, Z., Montello, A., Carter, C. D., Lempert, W. R., and Adamovich, I. V., 2013, "Measurements of Temperature and Hydroxyl Radical Generation/Decay in Lean Fuel–Air Mixtures Excited by a Repetitively Pulsed Nanosecond Discharge," Combust. Flame, **160**(9), pp. 1594–1608.
[27] Rousso, A., Yang, S., Lefkowitz, J., Sun, W., and Ju, Y., 2017, "Low Temperature Oxidation and Pyrolysis of n-Heptane in Nanosecond-Pulsed Plasma Discharges," Proc. Combust. Inst., **36**(3), pp. 4105–4112.
[28] Cheong, K.-P., Wang, G., Mi, J., Wang, B., Zhu, R., and Ren, W., 2018, "Premixed MILD Combustion of Propane in a Cylindrical Furnace With a Single Jet Burner: Combustion and Emission Characteristics," Energy Fuels, **32**(8), pp. 8817–8829.
[29] Yang, S., Nagaraja, S., Sun, W., and Yang, V., 2017, "Multiscale Modeling and General Theory of Non-Equilibrium Plasma-Assisted Ignition and Combustion," J. Phys. D: Appl. Phys., **50**(43), p. 433001.
[30] Tang, Y., Simeni Simeni, M., Frederickson, K., Yao, Q., and Adamovich, I. V., 2019, "Counterflow Diffusion Flame Oscillations Induced by ns Pulse Electric Discharge Waveforms," Combust. Flame, **206**, pp. 239–248.
[31] Wada, T., Lefkowitz, J. K., and Ju, Y., 2015, "Plasma Assisted MILD Combustion," 53rd AIAA Aerospace Sciences Meeting, Kissimmee, FL, Jan. 5–9.
[32] Ju, Y., Lefkowitz, J. K., Wada, T., Yang, X., Won, S. H., and Sun, W., 2015, "Plasma Assisted Combustion: Kinetic Studies and New Combustion Technology," 53rd AIAA Aerospace Sciences Meeting, Kissimmee, FL.
[33] Mardani, A., and Khanehzar, A., 2019, "Numerical Assessment of MILD Combustion Enhancement Through Plasma Actuator," Energy, **183**, pp. 172–184.
[34] Dally, B. B., Karpetis, A. N., and Barlow, R. S., 2002, "Structure of Turbulent Non-Premixed Jet Flames in a Diluted Hot Coflow," Proc. Combust. Inst., **29**(1), pp. 1147–1154.
[35] Mousavi, S. M., Kamali, R., Sotoudeh, F., Pourabidi, R., Karimi, N., and Jeung, I.-S., 2019, "A Comprehensive Investigation of Acoustic Power Level in a Moderate or Intense Low Oxygen Dilution in a Jet-in-Hot-Coflow Under Various Working Conditions," Aerosp. Sci. Technol., **93**, p. 105339.
[36] Lefkowitz, J. K., Guo, P., Rousso, A., and Ju, Y., 2015, "Species and Temperature Measurements of Methane Oxidation in a Nanosecond Repetitively Pulsed Discharge," Philos. Trans. R. Soc., A, **373**(2048), p. 20140333.
[37] Elkholy, A., Nijdam, S., van Oijen, J., and de Goey, L., 2017, "A New DBD Microplasma Burner for Measuring the Effect of Nanosecond Discharge on Burning Velocity of CH4-Air Flame at Atmospheric Pressure," 6th EUCASS Thematic Workshop: Fundamentals of Aerodynamic Flow and Combustion Control by Plasmas, Apr. 9–14, Saint Petersburg, Russia.
[38] Jidenko, N., Bourgeois, E., and Borra, J. P., 2010, "Temperature Profiles in Filamentary Dielectric Barrier Discharges at Atmospheric Pressure," J. Phys. D: Appl. Phys., **43**(29), p. 295203.
[39] Nozaki, T., Miyazaki, Y., Unno, Y., and Okazaki, K., 2001, "Energy Distribution and Heat Transfer Mechanisms in Atmospheric Pressure Non-Equilibrium Plasmas," J. Phys. D: Appl. Phys., **34**(23), pp. 3383–3390.
[40] Kappes, T., Schiene, W., and Hammer, T., 2002, *Energy Balance of a Dielectric Barrier Discharge Reactor for Hydrocarbon Steam Reforming*, University of Tartu, Estonia.
[41] Sadat, H., Dubus, N., Pinard, L., Tatibouet, J. M., and Barrault, J., 2009, "Conduction Heat Transfer in a Cylindrical Dielectric Barrier Discharge Reactor," Appl. Therm. Eng., **29**(5), pp. 1259–1263.
[42] Sadat, H., Dubus, N., and Tatibouët, J. M., 2012, "Temperature Runaway in a Pulsed Dielectric Barrier Discharge Reactor," Appl. Therm. Eng., **37**, pp. 324–328.
[43] Christo, F. C., and Dally, B. B., 2005, "Modeling Turbulent Reacting Jets Issuing Into a Hot and Diluted Coflow," Combust. Flame, **142**(1), pp. 117–129.

[44] Walker, R. W., 1990, "Free Radicals in Combustion Chemistry," Sci. Prog., **74**(2), pp. 163–187.
[45] Paul, P. H., and Najm, H. N., 1998, "Planar Laser-Induced Fluorescence Imaging of Flame Heat Release Rate," Symp. (Int.) Combust., **27**(1), pp. 43–50.
[46] Baukal, C. E., 2004, *Industrial Burners Handbook*, CRC Press, Boca Raton, FL.
[47] Lieuwen, T. C., and Yang, V., 2013, *Gas Turbine Emissions*, Cambridge University Press, Cambridge, New York.
[48] Krasnoperov, L., 2006, "Role of Formyl Radical (HCO) in Hydrocarbon Flames," Chem. Phys., **25**(10), pp. 13–17.
[49] Miller, J. A., Kee, R. J., and Westbrook, C. K., 1990, "Chemical Kinetics and Combustion Modeling," Annu. Rev. Phys. Chem., **41**(1), pp. 345–387.
[50] Warnatz, J., Maas, U., Dibble, R. W., and Warnatz, J., 1996, *Combustion*, Springer, New York.
[51] Nikolaou, Z. M., and Swaminathan, N., 2014, "Heat Release Rate Markers for Premixed Combustion," Combust. Flame, **161**(12), pp. 3073–3084.